ASTONJADRO

pISSN 2302-4240
eISSN 2655-2086

Volume 14, Issue 3, September 2025, pp.0893-0902
DOI: http://dx.doi.org/10.32832/astonjadro.v14i3.18400 http://ejournal.uika-bogor.ac.id/index.php/ASTONJADRO

Aeroelastic Heaving Response of a Cable-stayed Bridge Deck During Vortex Induced Vibration (Case Study of Suramadu Bridge)

I Gede Agung Shri Parta H, Bambang Supriyadi, Andreas Triwiyono

Department of Civil and Environmental Engineering, Universitas Gadjah Mada, Yogyakarta, INDONESIA

E-mail: igedeagungshripartah@mail.ugm.ac.id, bambang.supri@ugm.ac.id

| Submitted: December 06, 2024 | Revised: January 10, 2025 | Accepted: August 10, 2025 |

| Published: September 23, 2025 |

ABSTRACT

Aerodynamic phenomena poses risks for long-span cable-stayed bridge structures, nevertheless, the prevention method is often neglected on older bridges. The effort to reduce the risk and increase the aerodynamic performance of cable-stayed bridges mostly focuses on design and construction stages. This study attempts to improve aerodynamic performance by mitigating the aeroelastic heaving response of an existing bridge structure chosen as the subject, Suramadu Bridge. The approach is made by exploring different options applicable to already built bridges, such as the addition of fairings with varying shapes to modify the shape model of the bridge deck while maintaining the value of vertical and torsional stiffness. The study finds that there is relatively no increase in the lowest margin of critical vortex velocity of the bridge deck with fairing addition compared to the original bridge deck. The amplitude of oscillation caused by aerodynamic lift force is also fairly low since critical vortex velocity occurs in the range of 9.35-9.38 m/s. Upon increasing wind velocity up to the design wind speed of 37.8 m/s, there are significant differences in lift force and amplitude of oscillations. The shape model with the steepest fairing shows a significant decrease in amplitude, up to 35.6% lower than the original bridge deck, indicating a better aerodynamic stability. Meanwhile, the other two shape models show identical and higher amplitude compared to the original bridge deck.

Keywords: heaving response; shape model; frequency; lift force; amplitude.

INTRODUCTION

Climate change has challenged our understanding of wind behavior in the equatorial region. Tropical countries that lie at 23° latitude to the north and south of the equator line used to experience extreme wind velocity by the Coriolis Effect rarely. But lately, the formation of cyclones has increased significantly, causing extreme weather along with unusually high wind velocity to occur, posing risks to structures that are not designed to withstand such conditions. Thus the impact of wind and aerodynamic phenomena must be studied thoroughly to improve the design and maintenance of bridge structures.

Within Indonesia, several bridges are categorized as “special bridges” to differentiate them from “standard bridges” that are confined to short span - I girder or truss bridges. The special bridge category includes long-span - arch, cable-stayed, and suspension bridges [1]. As the name suggests, a special bridge requires more attention and detail in the design, construction, and maintenance. Special bridges hold more potential since they can reach a longer span while maintaining the whole structure to be cost-effective. However, as the span increases, so do the risks caused by the structural demands and the environmental effects. One risk often being neglected is the impact of dynamic wind on bridge structure and its aerodynamic phenomenon. The most well-known example is the collapse of Tacoma Narrows Bridge by self-induced excitation at a fairly low wind velocity, 17.8 m/s [2].

The impact of dynamic wind on a bridge structure referred to as aerodynamic phenomena and normally occurs in several stages. Vortex excitation or vortex-induced vibration (VIV) starts at the lowest velocity and should be expected to occur frequently during the service period of the bridge

[3]. Flutter or self-excited vibration occurs at a higher velocity, mainly marked by the coupling of bending and torsional frequency of the bridge. The last phenomenon that leads to the failure of a bridge structure is galloping, when self-excited vibration causes fatigue to the bridge structure [4]. Upon reaching a certain value marked as critical vortex velocity, wind velocity will conjure vortices around the deck of a bridge, thus causing VIV. Furthermore, if the natural frequency of the bridge matches with Karman vortex frequency, there are risks of structural instabilities. On a deck with lower torsional stiffness, the aspect ratio between the width and depth (B/H) of the bridge deck plays an important role [5]. With B/H less than 9.05, vertical and torsional VIV occurs simultaneously, and when B/H is between 9.05 to 11.96, VIV occurs separately.

Efforts have been made to increase the stability of long-span bridges such as to differentiate vertical and torsional frequency as much as possible, mainly by increasing the torsional stiffness of the bridge [6] Another approach is to ensure that the ratio of width and span (B/L) of the bridge deck is higher than 0.033. It has been found that B/L ratio of 0.033 and higher significantly reduces the risk of aerodynamic instabilities on frequent wind velocity [7]. The advantage of increasing bridge deck width is torsional stiffness will automatically improve too, thus lowering the risk of mode coupling. Another intricate method is dividing the bridge deck in the transversal direction, creating a wind vent in between two lanes of the service area of the deck. The division will separate the bride deck into two bluff bodies, shortening the possible turbulence length and further raising the margin of the wind velocity, causing VIV and flutter [8].

The methods aforementioned to reduce aerodynamic risks were only applicable during bridge design and construction periods. One method potentially applicable to existing bridge structures is the addition of fairing installed on the outer side of the bridge deck, thus changing the shape model of the deck [5]. This study aims to improve the aerodynamic performance of an existing bridge structure by analyzing parameters calculable in aeroelastic responses. Various degrees of fairing were used to get an idea of how wind velocity interacts with different shape models of a deck.

RESEARCH METHODS

This study is conducted numerically with the help of MIDAS Civil to model and analyze the vibration and response of the bridge structure. Open-source cloud-based software SimScale was also used to analyze the interaction between external airflow against a bridge deck shape model. The study starts with data collection process involving secondary sources from literatures. The data needed for modelling are bridge materials and general geometry arrangement. Bridge model created from available data is then analyzed to obtain the natural frequency and period of the structure. The analysis result is then used to predict vortex velocity. Environmental data is also needed to model the fluid dynamics analysis for the bridge model.

Bridge Modelling

Suramadu Bridge is currently the longest cable-stayed bridge in Indonesia. Suramadu Bridge consists of two parts, the approach bridge and the main bridge. The structural type of the main bridge is a cable-stayed bridge with a fan cable system, semi-H type pylon, and double cable planes. Two side spans of 192 m and a main span of 434 m composed the main bridge resulting in an overall length of 818 m. The general arrangement of the Suramadu Bridge is presented in Figure 1, which shown in half the total length of the bridge as the structure is identical.

In Figure 1, SC label stands for side-span cables and MC stands for main-span cables. In total, there are 140 stay cables arranged in two planes, each made of 7 mm wire strands. The typical space of two cables in the transversal direction is 12 m except for the two outermost side-span cables. One constraint group of cables consists of 35 individual cables, 17 side-span cables, and 1 additional cable in line with the pylon. The bridge deck was made of steel plates assembled into two box girders connected by I-section cross beams. Two additional DOFs added to the outer side of the box girder, from here onwards will be referred to as rib section. The total width of the bridge deck is 30 m and accommodates four traffic lanes and two motorway lanes. The cross-section of the bridge deck is presented in Figure 2.

ASTONJADRO
pISSN 2302-4240
eISSN 2655-2086
Volume 14, Issue 3, September 2025, pp.0893-0902
DOI: http://dx.doi.org/10.32832/astonjadro.v14i3.18400 http://ejournal.uika-bogor.ac.id/index.php/ASTONJADRO

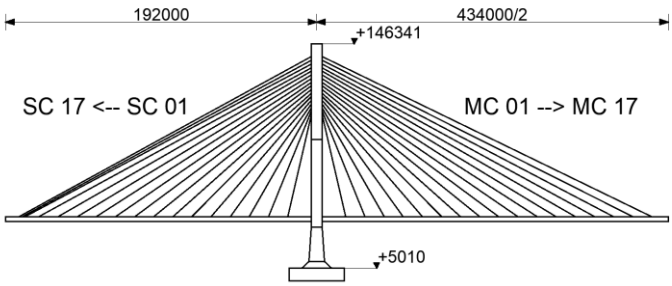

Figure 1. Typical bridge arrangement

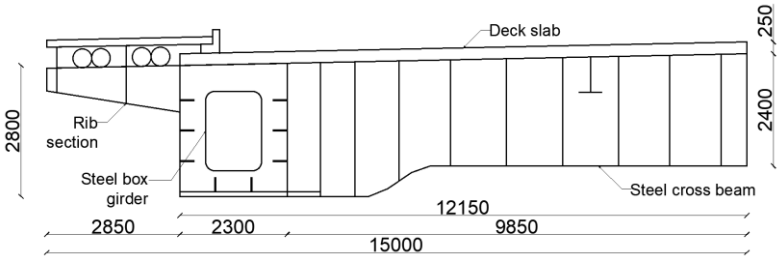

Figure 2. Half cross-section of the bridge deck

To account for the similarity of the bridge model and the real bridge, two aspects can be taken into consideration: the bridge's natural frequency and the pretension force of each stay cable. The data on natural frequency and pretension force were obtained from literature provided by Yadi [9].

There are three types of fairing to be added to the outer side of the bridge deck. Those are centered fairing with 21° angle (Model I), eccentric 11° angle fairing (Model II), and eccentric 29° angle fairing (Model III). These variations of fairing will simulate different shape factors in the 0.8-0.9 range [10]. The different shapes of fairings are shown in Figure 3. The fairings will be made with 5 mm Q345q steel plates, identical to the original bridge deck material. The fairing is not modeled to receive load, rather it is made just to divert the flow of wind in lateral angle of attack.

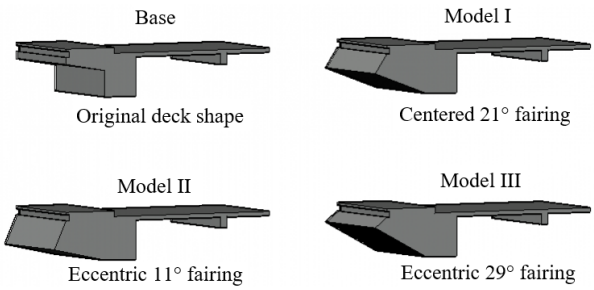

Figure 3. Bridge deck with different fairings

Critical Velocity

The mechanic of flow separation on the bridge deck is tied to the bluffness ratio and Reynolds number. The Bluffness of a bridge deck will dictate the speed of the separated flow around the body, the intensity of vortices formation, and the risk of flow reattachment [11]. Reynolds number, R_e portrays the overall stability of the body, as expressed in Equation (1).

$$\mathrm{Re}=\frac{U\times L}{\upsilon} \tag{1}$$

where U is the mean wind velocity around the body, L is the reference length of the body, and ν is the kinematic viscosity of the fluids. Reynolds number can be divided into three regions, sub-critical ($Re < 5\times10^5$), super-critical ($5\times10^5 < Re < 5\times10^6$), and trans-critical ($Re > 5\times10^6$) [5]. The sub-critical region is the most unfavorable region due to the risk of instabilities caused by flow reattachment occurring close to the body. The forming of the vortices around the bridge deck might excite the structure, causing it to oscillate. Oscillation will happen if the vortex frequency matches the vertical bending frequency of the structure [19], represented by Strouhal number, St, expressed in Equation (2).

$$n_s = St\frac{U}{D} \tag{2}$$

where n_s is the vortex frequency and D is the bridge deck depth. Therefore, by substituting the vortex frequency value with the bending frequency of the structure, the critical velocity can be obtained.

Two assumptions are being used for the empirical Strouhal number. The first is the S_t value of 0.20 which is based on the supposition that wind flow comes from both sides of the deck. Second, the S_t value of 0.10 under the idealized assumption that the wind flow only comes from one side of the deck. It must be noted that design wind velocity also has to be accounted for. Based on the empirical method, the design wind velocity (U_d) is calculated using the formula in Equation (3).

$$U_d = \left(\frac{\delta_B}{10}\right)^{0.16}\left(\frac{Z}{\delta_A}\right)^{0.12} U_{10} \tag{3}$$

where δ_A and δ_B are the wind gradient with values of 350 m and 300 m respectively. While Z is the elevation where the design wind velocity impacts, which is 42.35 m, and V_{10} is the highest recorded mean wind velocity at 28.3 m/s. Based on those values, the calculated design wind velocity, U_d = 37.8 m/s.

Computational Fluid Dynamics

Computational fluid dynamics (CFD) is one way to obtain a depiction of fluid behavior upon contact with the structure. The aerodynamic modeling is based on wind tunnel simulation [12] and Ahmed body simulation [13]. Concerning the Reynolds number of the system, the CFD simulation is based on the High Reynolds Number (HRN) function approach. The CFD simulation model is presented in Figure 4.

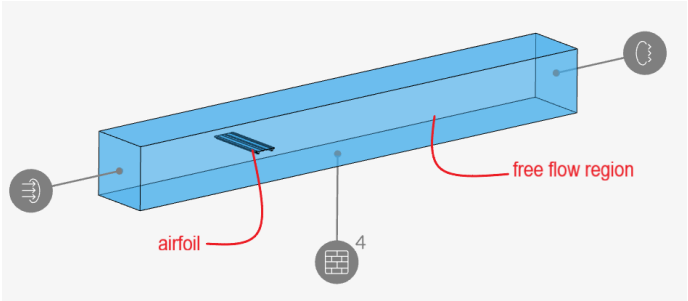

Figure 4. CFD model for aerodynamic simulation

Fluid in the simulation is air in the open space, modeled as external flow around a body. Moreover, the critical velocity and the design velocity to be checked are far below 100 m/s, therefore air is treated as an incompressible fluid. As an incompressible fluid, k-ω SST turbulence model was the most suitable as the model accounts for the time history effect of the wind during the simulation [14], [15].

pISSN 2302-4240
eISSN 2655-2086
Volume 14, Issue 3, September 2025, pp.0893-0902
DOI: http://dx.doi.org/10.32832/astonjadro.v14i3.18400 http://ejournal.uika-bogor.ac.id/index.php/ASTONJADRO

Aeroelastic Response of the Structure

Aeroelastic response in heaving direction is normally expressed as the amplitude of oscillations and acceleration. The function of amplitude (u) and acceleration ($\ddot{u}$) is presented in Equation (4) and Equation (5), respectively.

$$u = \frac{\pi}{\delta}\frac{F_L}{m}\hat{u}_{static} \tag{4}$$

$$\ddot{u} = 4\pi^2 f_b^2 u \tag{5}$$

where δ is the logarithmic decrement of 0.05, F_L is the generated lift force in the lateral length of the deck, m is the mass of the deck, and $\hat{u}_{static}$ is the maximum deformation of the deck under dead loads and 25% uniformly distributed live load, and f_b is the bending frequency [16]. The amplitude limitation in the vertical direction should not exceed $u_{max} = 0.04/f_b$ [5]. Lift force is calculated based on the wind velocity difference obtained from CFD analysis. Flow separation caused by the body will result in differences in wind velocity above and below the body. Lower wind velocity gives higher pressure, while higher wind velocity gives lesser pressure. Therefore, when the wind velocity above the deck is faster than the wind velocity below the deck, lift happens [17], [18]. The formula for lift (F_L) is shown in Equation (6).

$$F_L = \frac{1}{2}\rho(U_1^2 - U_2^2)(C_L) \tag{6}$$

RESULT AND DISCUSSION

Bridge Model Similarity

Modal analysis done on the bridge model showed good agreement with the source data. The model follows a typical cable-stayed bridge mode shape with vertical bending as the first mode shape. Mode shape and frequency of the model bridge compared to the source data presented in Table 1.

Table 1. Mode shape and frequency of the bridge

Mode	Mode Shape	Experiment result* (Hz)	Numerical result (Hz)
1	S-vertical bending	0.280	0.278
2	S-transversal bending	0.285	0.291
3	A-vertical bending	0.364	0.340
4	A-transversal bending	0.549	0.454
5	Torsional (1st order)	0.570	0.512

*) experimental data [9]

The proposed mode shape frequency achieves the expected result. The fairings weren't designed as structural elements, thus the result showed no significant increase in vertical and torsional frequency in the model with added fairings. A comparison of the frequency of different bridge models is presented in Table 2.

Table 2. Vertical and torsional frequencies of different models

Model	Vertical (Hz)	Torsional (Hz)
Base model	0.278	0.512
Model 1 (21° fairing)	0.279	0.562
Model 2 (11° fairing)	0.280	0.569
Model 3 (29° fairing)	0.279	0.554

Generated Lift

Applying the calculated velocity as free flow velocity for the duration of 1000 s, the velocity magnitude around the body then could be obtained. In Figure 5 it is shown that flow separation happens in the form of a boundary layer around the deck, marked by blue-green color, causing a difference of velocity. The velocity difference is taken by probe point sampling to be used in the lift force (F_L) equation. The maximum lift force of each bridge deck model variation is presented in Table 3.

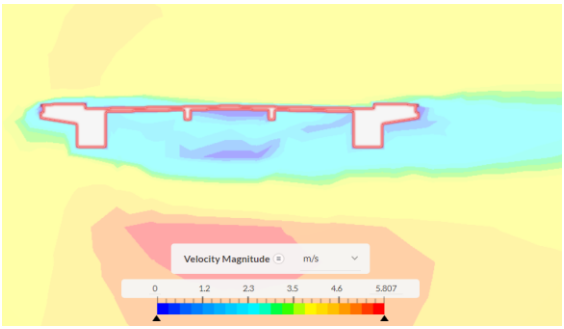

Figure 5. Flow separation around the original deck section

Table 3. Critical wind velocity and lift force of the deck

Model	U_{cr}	U_{cr} flow (m/s)		ρ	F_L static	F_L max	Lift
	(m/s)	Top (U_1)	Bottom (U_2)	(kg/m^3)	(Pa)	(Pa)	(kN/m)
St = 0.20							
Base	4.67	3.73	1.14	1.225	1.47	0.85	25.50
Model 1 (21°)	4.67	5.01	2.83	1.225	1.47	1.15	36.50
Model 2 (11°)	4.69	4.88	1.27	1.225	1.48	1.50	47.42
Model 3 (29°)	4.67	4.35	0.42	1.225	1.47	1.26	40.04
St = 0.10							
Base	9.35	8.93	2.18	1.225	5.89	5.05	151.58
Model 1 (21°)	9.35	10.07	5.77	1.225	5.89	4.59	145.47
Model 2 (11°)	9.38	9.73	1.38	1.225	5.93	6.25	198.13
Model 3 (29°)	9.35	8.58	1.08	1.225	5.89	4.88	154.74
Design wind velocity = 37.8 m/s							
Base	37.80	36.59	-9.36	1.225	96.27	84.30	2529.03
Model 1 (21°)	37.80	37.9	11.97	1.225	96.27	87.13	2761.85
Model 2 (11°)	37.80	39.3	10.97	1.225	96.27	95.95	3041.68
Model 3 (29°)	37.80	29.42	5.71	1.225	96.27	56.12	1778.96

Aeroelastic Heaving Response

To obtain the numerical value of the aeroelastic response, the maximum deformation of the deck or ustatic must be first calculated. The loading pattern used follows the standard set in SNI 1725:2016. Using the lift force value in Table 3, the mass of the deck (m), and the deformation value ($\hat{u}_{static}$), the amplitude of oscillation and acceleration then can be obtained. The amplitude of oscillation and acceleration are presented in Table 4. The calculated amplitude result for critical flutter velocity and the design wind velocity show a similar pattern. Model 3 consistently generates lower lift force and amplitude response than the original bridge deck or Base model. Also considering the additional mass of the bridge deck due to the addition of fairings, model 3 needed the least material (1.03%) out of the three proposed variations (Model 1 = 3.82%; Model 2 = 1.15%).

pISSN 2302-4240
eISSN 2655-2086
Volume 14, Issue 3, September 2025, pp.0893-0902
DOI: http://dx.doi.org/10.32832/astonjadro.v14i3.18400 http://ejournal.uika-bogor.ac.id/index.php/ASTONJADRO

Table 4. The amplitude of oscillation and acceleration of the deck

Model	f_b (Hz)	Ref. length (m)	F_L flow (Pa)	$\hat{u}_{static}$ (mm)	m (kN/m)	u (mm)	$\ddot{u}$ (m/s^2)
St = 0.20							
Base	0.279	30.0	0.85	223.801	404.846	0.886	0.003
Model 1 (21°)	0.279	31.7	1.15	211.910	420.350	1.156	0.004
Model 2 (11°)	0.280	31.7	1.50	211.385	409.501	1.538	0.005
Model 3 (29°)	0.279	31.7	1.26	212.083	409.023	1.304	0.004
St = 0.10							
Base	0.279	30.0	5.05	223.801	404.846	5.265	0.016
Model 1 (21°)	0.279	31.7	4.59	211.910	420.350	4.608	0.014
Model 2 (11°)	0.280	31.7	6.25	211.385	409.501	6.426	0.020
Model 3 (29°)	0.279	31.7	4.88	212.083	409.023	5.041	0.015
Design wind velocity = 37.8 m/s							
Base	0.279	30.0	84.30	223.801	404.846	87.843	0.270
Model 1 (21°)	0.279	31.7	87.13	211.910	420.350	87.482	0.269
Model 2 (11°)	0.280	31.7	95.95	211.385	409.501	98.653	0.305
Model 3 (29°)	0.279	31.7	56.12	212.083	409.023	57.957	0.178

Using the generated lift value throughout the 1000 s duration of the CFD analysis run, the time history load case can then be designed. The heaving response was taken from the node with the highest displacement value. Based on the amplitude limitation, the displacement caused by the heaving response should not exceed 143.369 mm. The heaving response graph of critical vortex velocity and design wind velocity are presented in Figure 6 and Figure 7.

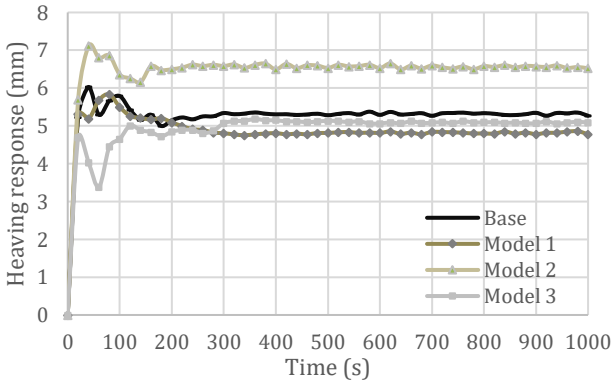

Figure 6. Heaving response of the critical vortex velocity

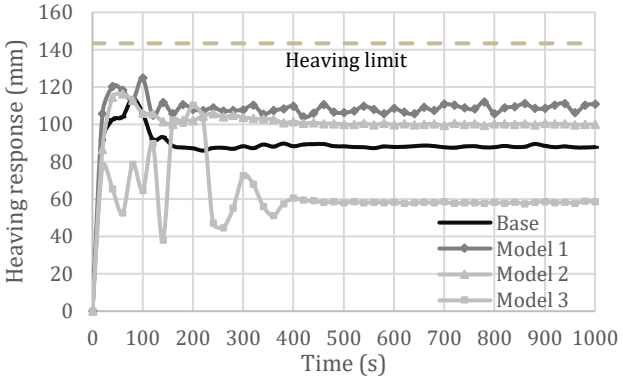

Figure 7. Heaving response of the design wind velocity

The comparison of the calculated amplitude value and the heaving response is presented in Table 5. The result shows that heaving responses overall are higher than the calculated amplitude value. The differences are much more noticeable when the analysis run are still in the earlier stage and the free flow velocity hasn't stabilized.

Table 5. Amplitude and response comparison

Model	Amplitude max. (mm)	Heaving max. (mm)
Critical vortex velocity		
Base	5.265	6.030
Model 1 (21°)	4.608	5,833
Model 2 (11°)	6.426	7.116
Model 3 (29°)	5.041	5.184
Design wind velocity		
Base	87.843	113.854
Model 1 (21°)	87.482	124.764
Model 2 (11°)	98.653	116.316
Model 3 (29°)	57.957	110.197

The heaving response shows a spike in the earlier stage of the analysis. Then as the free flow duration increases, the deck will oscillate in about the same value as the amplitude mentioned in Table 4. Out of the three variations of fairing shape that were proposed, Model 3 with 29° fairing consistently shows a lower spike and lower overall displacement compared to the original bridge deck shape. The result of this research correspondent with previous study of π-section bridge deck with various fairing addition [20], which shows a bridge deck with steeper fairing shows lower value of amplitude upon reaching higher wind velocity in vortex shedding region. Even so, during the lower velocity near critical vortex velocity, there are no significant differences between different deck shapes. The heaving response of design wind velocity also complies with the designated heaving limit.

CONCLUSION

The effect of fairing shape model variations towards aeroelastic response has been evaluated in this study. The addition of fairing does not tamper with the overall stiffness of the bridge deck, thus maintaining the bending frequency at the same value of 0.278-0.280 Hz. Based on the CFD simulation, Model 3 (29° inclination) with the fairing more inclined toward the upper side of the deck able to generate less lift force than the original shape of the deck, at about 56.119 Pa compared to 84.301 Pa. The aeroelastic response also shows a good agreement with the calculated amplitude of oscillations. Model 3 shows a consistently better result compared to the original deck shape both in critical vortex velocity and design wind velocity. This can be observed from the displacement value as a result of the oscillation. Model 3 shows a peak displacement value of 110.854 mm and oscillation amplitude of about 57-58 mm, less than the original deck shape with 113.854 of peak displacement and 87-89 mm of amplitude. This study is expected to bring more consideration to

pISSN 2302-4240
eISSN 2655-2086
Volume 14, Issue 3, September 2025, pp.0893-0902
DOI: http://dx.doi.org/10.32832/astonjadro.v14i3.18400 http://ejournal.uika-bogor.ac.id/index.php/ASTONJADRO

long-span cable-stayed bridge design even in regions with low recorded wind velocity. The results of this study can be used as a framework to design safer and more stable cable-stayed bridges in the future.

REFERENCES

[1] Hidayat, A., Supriyadi, B., & Triwiyono, A. (2021). Analisis Stabilitas Jembatan Cable-Stayed Prestressed Box Girder Dengan Variasi Rasio Bentang Terhadap Lebar Jembatan. *Prosiding CEEDRiMS 2021*, 99–104.

[2] Kimura, K. (2016). Wind loads. *Innovative Bridge Design Handbook: Construction, Rehabilitation and Maintenance*, 47–59. https://doi.org/10.1016/B978-0-12-823550-8.00031-7

[3] Poddaeva, O. I., Fedosova, A. N., & Churin, P. S. (2020). The influence of the structural vibrations' logarithmic decrement on its stability in the event of vortex excitation. *IOP Conference Series: Materials Science and Engineering*, *913*(4). https://doi.org/10.1088/1757-899X/913/4/042069

[4] Wu, L., Woody Ju, J., Zhang, J., Zhang, M., & Li, Y. (2023). Vibration phase difference analysis of long-span suspension bridge during flutter. *Engineering Structures*, *276*(December 2022), 115351. https://doi.org/10.1016/j.engstruct.2022.115351

[5] Bai, H., Li, R., Xu, G., & Kareem, A. (2021). Aerodynamic performance of Π-shaped composite deck cable-stayed bridges including VIV mitigation measures. *Journal of Wind Engineering and Industrial Aerodynamics*, *208*. https://doi.org/10.1016/j.jweia.2020.104451

[6] Andersen, M. S., Johansson, J., Brandt, A., & Hansen, S. O. (2016). Aerodynamic stability of long span suspension bridges with low torsional natural frequencies. *Engineering Structures*, *120*, 82–91. https://doi.org/10.1016/j.engstruct.2016.04.025

[7] Supriyadi, B., Siswosukarto, S., Masagala, A. A., & Hadjoh, I. E. S. (2017). The Effect of Deck Width Addition Toward Stability of Cable Stayed Bridge: Case Study of Siak Sri Indrapura Bridge, Riau. *MATEC Web of Conferences*, *103*. https://doi.org/10.1051/matecconf/201710309010

[8] Morgenthal, G., & Yamasaki, Y. (2011). Aerodynamic behaviour of very long cable-stayed bridges during construction. *Procedia Engineering*, *14*, 1463–1471. https://doi.org/10.1016/j.proeng.2011.07.184

[9] Yadi, S., Suhendro, B., Priyosulistyo, H., & Aminullah, A. (2018). Shake table test of floating cable-stayed bridge under earthquake excitation during construction with balanced cantilever method. *International Journal of Civil Engineering and Technology*, *9*(11), 2063–2081.

[10] Dyrbye, C., & Hansen, S. O. (1997). Wind Loads on Structures. In *Wind Loads on Structures*. https://doi.org/10.1680/ijoti_1950_12863

[11] Abbas, T., Kavrakov, I., & Morgenthal, G. (2017). Methods for flutter stability analysis of long-span bridges: A review. *Proceedings of the Institution of Civil Engineers: Bridge Engineering*, *170*(4), 271–310. https://doi.org/10.1680/jbren.15.00039

[12] Subagyo. (2018). Assessment of static aerodynamic stability bridge with computational and experimental method. *Journal of Physics: Conference Series*, *1130*(1). https://doi.org/10.1088/1742-6596/1130/1/012009

[13] Aguerre, H. J., Gimenez, J. M., Escribano, F., & Nigro, N. M. (2024). Aerodynamic study of a moving Ahmed body by numerical simulation. *Journal of Wind Engineering and Industrial Aerodynamics*, *245*(March 2023), 105635. https://doi.org/10.1016/j.jweia.2023.105635

[14] Townsend, J. F., Xu, G., & Jin, Y. (2024). Roughness constant selection for Atmospheric Boundary Layer simulations using a k – ω SST turbulence model within a commercial CFD solver. *Preprint*, *1*(1), 100005. https://doi.org/10.1016/j.awe.2024.100005

[15] Younoussi, S., & Ettaouil, A. (2024). Calibration method of the k-ω SST turbulence model for wind turbine performance prediction near stall condition. *Heliyon*, *10*(1), e24048. https://doi.org/10.1016/j.heliyon.2024.e24048

[16] Walther, R., Houriet, B., Isler, W., Klein, J. F., & Moia, P. (1999). Cable Stayed Bridges Second Edition. In *Thomas Telford Publishing, Heron Quay, London*.

[17] Simiu, E., & Yeo, D. (2019). *Wind Effects on Structures Modern Structural Design for Wind* (4th ed., Vol. 19). John Wiley & Sons.

[18] Svensson, H. (2012). *CABLE-STAYED BRIDGES 40 Years of Experience Worldwide* (1st ed.). Wilhelm Ernst & Sohn, Verlag für Architektur und technische Wissenschaften GmbH & Co. KG.

[19] Churin, P., & Fedosova, A. (2019). Aerodynamic Stability of Bridge Structures. *IOP Conference Series: Materials Science and Engineering*, *661*(1). https://doi.org/10.1088/1757-899X/661/1/012050

[20] Bird, R. B., Stewart, W. E., & Lightfoot, E. N. (2001). *Transport Phenomena 2nd Edition* (2nd ed.). John Wiley & Sons.